ISBN: 978-3-95450-234-9 ISSN: 2673-5504 doi:10.18429/JACoW-SRF2023-FRIBA07

STATUS OF THE SLAC/MSU SRF GUN DEVELOPMENT PROJECT*

S. Miller†, Y. Al-Mahmoud, W. Chang, Y. Choi, C. Compton, X. Du, K. Elliot, W. Hartung, J. Hulbert, S.-H. Kim, T. Konomi, D. Morris, M. Patil, L. Popielarski, K. Saito, A. Taylor, B. Tousignant, J. Wei, J. Wenstrom, K. Witgen, T. Xu
Facility for Rare Isotope Beams, Michigan State University, East Lansing, MI, USA
C. Adolphsen, R. Coy, F. Ji, M. Murphy, J. Smedley, L. Xiao
SLAC National Accelerator Laboratory, Menlo Park, CA, USA
J. Lewellen, Los Alamos National Laboratory, Los Alamos, NM, USA
M. Kelly, T. Petersen, P. Piot, Argonne National Laboratory, Lemont, IL, USA
A. Arnold, S. Gatzmaga, P. Murcek, R. Xiang, J. Teichert
Helmholtz-Zentrum Dresden-Rossendorf, Dresden, Germany

Abstract

The Linac Coherent Light Source II High Energy project at SLAC includes the construction of a low-emittance injector (LEI) and a superconducting quarter-wave resonator (QWR) at 185.7 MHz. Several alternatives to a superconducting radio frequency (SRF) QWR gun were considered for the LEI, including normal-conducting RF guns evolved from the LCLS-II gun design. Compared to normal-conducting designs, the combination of an intrinsically outstanding vacuum environment (for cathode lifetime), and the potential for a larger ultimate performance envelope, led to the decision to pursue development of the QWR-SRF gun. A prototype gun is currently being designed and fabricated at the Facility for Rare Isotope Beams at Michigan State University. This paper presents performance goals for the new gun design, an overview of the prototype development effort, status, and future plans including fabrication.

INTRODUCTION

In order to increase the electron beam energy to 8 GeV, Linac Coherent Light Source II High Energy (LCLS-II-HE) will construct a low-emittance injector (LEI) in a new tunnel [1, 2]. The beam source for the LEI will utilize a superconducting radio frequency photo-injector (SRF-PI). To mitigate the technical risk in adopting this approach, the LCLS-II-HE project proposed a 4-year R&D program to design, construct, and test a 185.7 MHz QWR SRF gun [3]. The goal of this R&D program is to demonstrate stable continuous wave (CW) operation with a cathode gradient of at least 30 MV/m. For the RF cavity, a major design criterion for the cavity is to achieve a low peak surface to cathode field ratio with consideration to field emission and multipacting. Two versions of the RF cavity are to be manufactured; one with a cathode plug port and one without. The latter will be tested initially to verify the cavity performance independent of the complications arising from the stalk and plug assembly. The Fundamental Power Coupler (FPC) is designed to be multipacting and field emission free, and not produce significant asymmetric fields in the cavity. The cavity tuner is to be designed to ensure the gun operates at the nominal frequency within the detuning budget. The cathode is to be designed to provide an RF short while minimizing the heat load to the helium bath. The emittance compensation solenoid is designed to be close to the SRF-PI anode and has transverse adjustability to meet alignment specifications. A SRF-PI cryomodule has been developed by Facility for Rare Isotope Beams (FRIB) and its collaborative partners with the aforementioned specifications utilizing a 185.7 MHz quarter-wave resonator (QWR) and a cathode system. Table 1 displays the scope of the collaborators for the project. Table 2 gives the performance parameters associated with the SRF-PI.

Table 1: The Scope of the Collaborative Project Undertaken by FRIB, ANL, HZDR, and SLAC

Scope	FRIB	ANL	HZDR
Project Management	✓		
Cryomodule Design	✓	✓	
Magnet Design and Testing	✓		
Cathode Stalk Design, Fab, Testing	✓	✓	
Load-lock, Insertion/Transport			✓
Cathode Stalk Particulate Testing			✓
Cryomodule Procurement/Assy	✓		
Load-Lock Procurement/ Assy	✓		
Cavity Processing and Cold Testing	✓	✓	
Integrated Cavity Test (Tuner/FPC)		✓	
Cavity Bunker Test	✓		

* Work supported by the Department of Energy under Contract DE-AC02-76SF00515
† millers@frib.msu.edu

ISBN: 978-3-95450-234-9 ISSN: 2673-5504 doi:10.18429/JACoW-SRF2023-FRIBA07

Table 2: SRF-PI Cryomodule Performance Parameters [3]

Parameter	Units	Value
Operating Temperature	K	4.2
Cavity Frequency at 4.2 K, 1 bar	MHz	185.7
Cathode Gradient (Nominal/Maximum Operating)	MV/m	> 30/35
Integrated E_z Field at 30 MV/m Gradient	MV	> 1.6
Captured Dark Current at 30 MV/m Gradient	nA	< 10
Distance from Cathode to Anode*	mm	70
Length of Solenoid Magnetic Yoke*	mm	124
Exit Beam Pipe Radius	mm	20
Cavity Q_0		> 1 x 10^9
RF Coupler Q_{ext}*		10^7
Static Heat Load at 4.5 K	W	< 25
Cavity Vacuum Pressure at Room Temperature	torr	< 1 x 10^{-9}
Helium Vessel Leak Rate at Room Temperature	torr-liter/sec	< 1 x 10^{-7}

*SLAC Design Values

CHALLENGES AND LESSONS LEARNED FROM EXISTING SYSEMS

Multiple challenges existed in the development of the SRF-PI cryomodule [4]. One challenge is to achieve the cathode field of 30 MV/m, which is significantly higher than existing SRF-PI systems have previously achieved during operation. Another challenge is to avoid field emission and multipacting which has been problematic to other systems. An additional challenge is the prevention of cavity degradation during cathode exchanges and the cathode operation at different temperatures. Additional design and development challenges are summarized in Table 3 along with their mitigation strategies.

CRYOMODULE DESIGN

The SRF-PI cryomodule design is complete and is shown in Figure 1. The FRIB cryomodules are based on a bottom-supported design which is optimized for mass-production and efficient precision-assembly. A similar design approach has been utilized on the SRF-PI cryomodule as shown in the timeline in Figure 2. Figure 3 displays the subsystem break down of the SRF-PI cryomodule.

Table 3: Challenges and Lessons Learned from Existing Projects - Mitigation Strategies Are Listed

Challenge	Development/Validation Impact
Field Emission Limits Performance and Produces Dark Current	• Add Rinse Ports • Make Cathode System as Clean as Possible • Make FPC Adjustable for High Peak Power Pulsed Processing • Plasma Processing if Needed
Multipacting Limit Performance	• DC Dias for Cathode Stalk and FPC • Design Systems for MP Avoidance • Apply FRIB Conditioning Experience
Auxiliaries: Couplers and Tuners are Critical Elements	• Existing Gun Projects Developed Unique Solutions: Dedicated Development • Adapt Proven Technology where Possible
Cathode and RF Choke Critical Performance	• Careful Design • Extra RF Pickup in Choke • Sub-System Testing, • Iteration as Needed
FPC on Beam Port: Complex System and Downstream Focusing	• Separate Off-Axis Port for FPC
RF Pickup on Beam Port Results in Systematic RF Amplitude Error	• Pickup Loop in Rinse Port

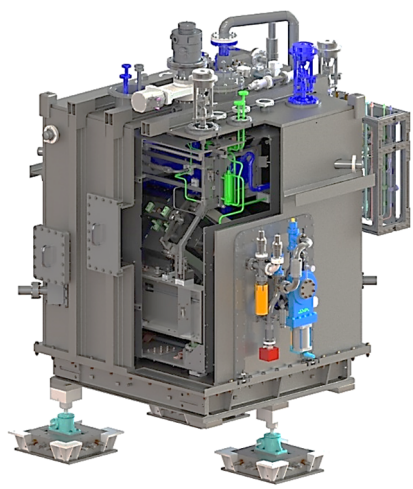

Figure 1: SRF-PI cryomodule bottom-up design.

ISBN: 978-3-95450-234-9 ISSN: 2673-5504 doi:10.18429/JACoW-SRF2023-FRIBA07

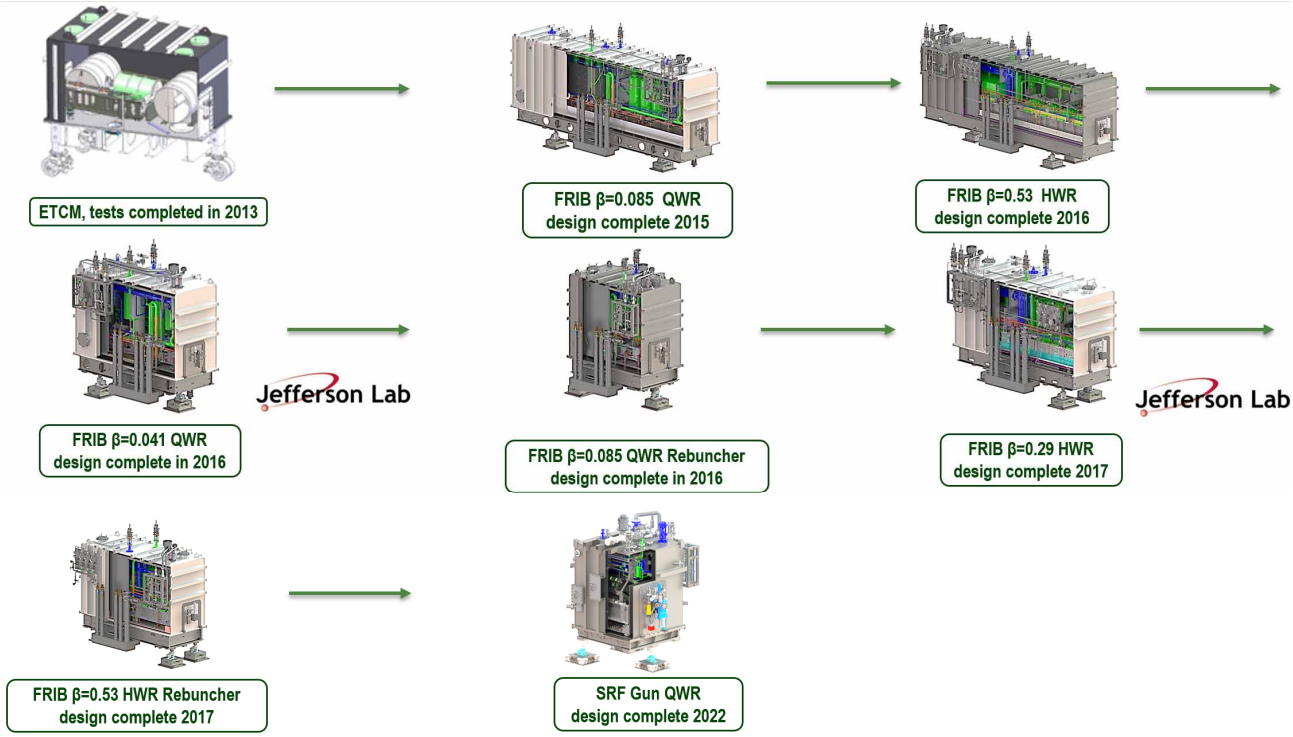

Figure 2: FRIB and SRF-PI cryomodule design timeline.

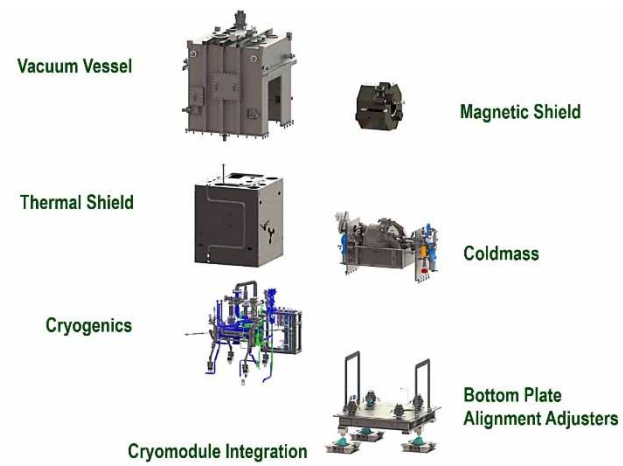

Figure 3: Sub-Systems of FRIB cryomodule design. Supported off the bottom plate is the coldmass system, where the resonator is protected by local magnetic shielding (right). The cryogenic system attaches to the coldmass. All assemblies are encapsulated by the thermal shield and vacuum vessel (left).

Superconducting Resonator

Figure 4 displays the SRF-PI 185.7 MHz quarter-wave resonator. Beam dynamic studies were performed with the accelerating gap distance of 70 mm with a beam pipe diameter of 40 mm [5]. The inner-conductor region around the cathode was originally based on the WiFEL gun geometry. This design was to minimize transverse field at the cathode and E-field enhancement [6]. Figure 5 displays the options that were considered for the 185.7 MHz quarter wave resonator design which were dependent on the short plate radius. A large-radius elliptical blend defines the anode region which reduces the strength of the potential low-field multipacting barriers. The short plate design was heavily investigated for the effect on the radius (R) as shown in Figure 5. Several factors were considered such as r/Q, G, Epeak, Bpeak, and multipacting strength. The investigation concluded that a larger short plate radius is preferred; improving the aforementioned factors. A radius of 75 mm was selected which balanced considerations about the mechanical stiffness of the inner conductor against pressure sensitivity and Lorentz force detuning (LFD).

Figure 4: SRF-PI 185.7 MHz quarter wave resonator.

ISBN: 978-3-95450-234-9 ISSN: 2673-5504 doi:10.18429/JACoW-SRF2023-FRIBA07

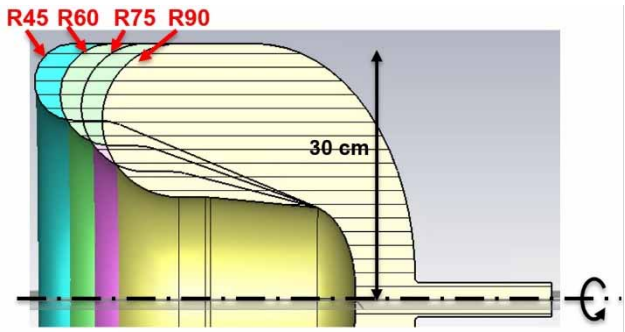

Figure 5: Cavity shapes for design consideration which are dependent on the short plate radius (R) [5].

With the optimal cavity shaped selected, beam, RF, and rinse ports were added. The E and B-field were checked with these additions as shown in Figure 6 and Figure 7. With the additions the ports the maximum B-field is located at the transitions of the short plate rinse ports as shown in Figure 7; however, since the maximum B-field if 52.9 mT, this moderate level did not warrant further efforts to enlarge the blending radii of the port to the shorting plate.

The helium vessel jacket which is shown in Figure 4, was optimized for several parameters. The helium vessel jacket cavity was designed in accordance with the ASME BPVC Section VIII, Division-2 [7]. The jacket was designed to minimize the frequency sensitivity to the helium bath pressure. The helium vessel material is Grade 2 Titanium to minimize cooldown frequency shifts as it will closely match the thermal contraction from the niobium cavity.

The complete list of cavity parameters is shown in Table 4. This table lists mechanical parameters such as tuning sensitivity and force. The frequency tuning range of the cavity is required to be 60 kHz, which will require 8.4 kN of tuning force. Additionally, the LFD values are listed in Table 4. It is important to note that the LFD is normalized to the stored energy of 1 J. The frequency shifts expected from the LFD are comparable to the FRIB half-wave resonators in which the performance was satisfactory [5]. Finally, the table also contains the mechanical modes of the cavity. As shown, the lowest cavity mode is 157 Hz which is sufficiently clear of resonant modes from electronics and those associated with the cryomodule.

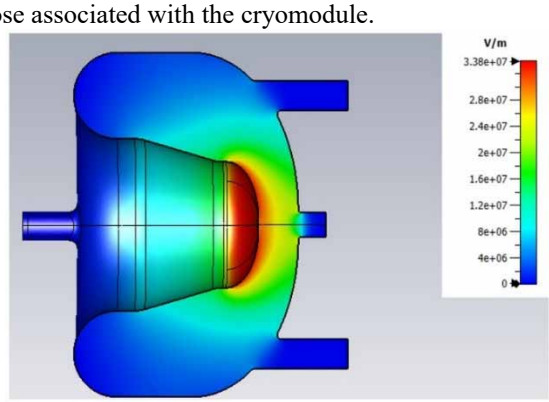

Figure 6: E-field results. E-field at Ec = 30 MV/m, Epeak = 33.7 MV/m.

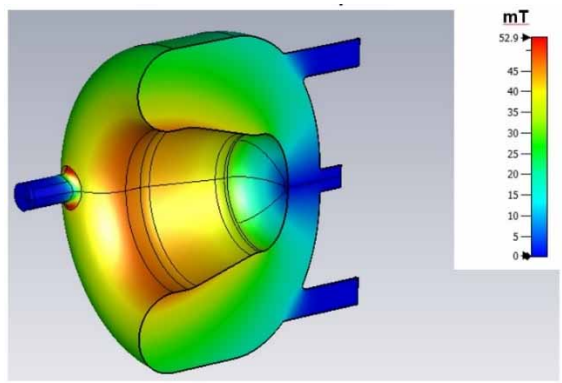

Figure 7: B-field results. B-field at Ec = 30 MV/m, Bpeak = 52.9 mT [5].

Table 4: SRF-PI 185.7 MHz Quarter-Wave Resonator Parameters [5]

Cavity Parameters	Value
f0 (MHz)	185.75
Geometry Factor (Ω)	84.5
Quality factor Q0 @ 4.4 K(1)	1.3 x 10^9
r/Q (Ω)	131
Ec (MV/m)	30
Stored Energy U (J)	21.4
Bpeak (mT)	52.9
Epeak (MV/m) with cathode	33.7
Cavity wall dissipation power Pw(1) (W)	20
Gap Voltage V0(2) (MV)	1.81
Accelerating voltage Vacc (β=1) (MV)	1.80
df/dP (Hz/Torr)	-3.95
df/dx (kHz/mm)	-435
dF/dx (kN/mm)	44.6
Tuning Force: 60 kHz, 15 psi, 4 K (kN)	8.4
LFD (Hz/J)	-29
Modes 1-3 (Hz)	157, 182, 191

Superconducting Solenoid Package

The emittance compensation solenoid will be utilized for the compensation of adverse space charge effects on the emittance of the electron beam [8]. The solenoid contains two sets of windings that can be independently powered in addition to bucking coils to minimize the fringe field at the resonator surface. The package also contains dipole and quadrupole coils to correct field errors due to misalignment and fabrication imperfections. The solid coil layout is shown in Figure 8 Adjustors are built into the solenoid package mounts to allow for adjustment within +/0.2 mm.

ISBN: 978-3-95450-234-9 ISSN: 2673-5504 doi:10.18429/JACoW-SRF2023-FRIBA07

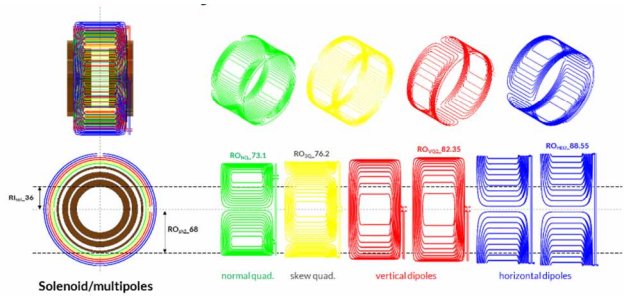

Figure 8: Solenoid coil layout [8].

Fundamental Power Coupler

The SRF-PI cryomodule will utilize an Argonne National Laboratory FPC design which was validated on the PIP-II half-wave resonators [9]. Figure 9 displays the FPC. This FPC contains a cold window, transition, and warm window. The FPC will be installed on off-axis port to reduce the impacts of potential particulate contamination on resonator operation. The FPC will utilize a 6 kW RF SSA power source and is designed to be multipacting free with a +200 V DC bias.

Figure 9: Fundamental power coupler for SRF-PI.

Resonator Tuner

The SRF-PI cryomodule will utilize a Fermi National Laboratory tuner design which was validated on the PIP-II single spoke resonators [10]. Figure 10 depicts the tuner as installed on the resonator. The tuner will provide unidirectional tuning to the cathode port. The design utilizes a stepper based slow tuner and piezo actuator based fast tuner. The fast tuning piezo actuators have resolution of under 1 Hz and are fast enough to track slow changes in the cavity frequency.

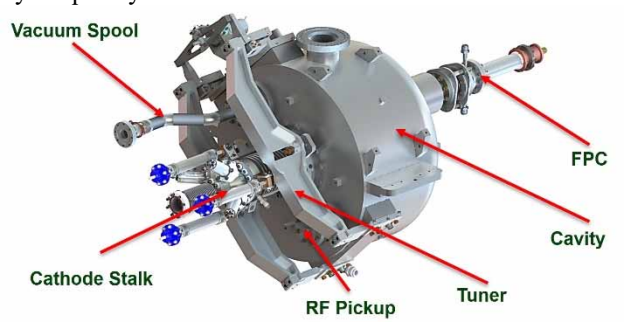

Figure 10: Tuner as installed on the resonator for the SRF-PI cryomodule.

Cathode Stalk

The cathode stalk for the SRF-PI is one of the most critical and challenging components to develop. The performance and cleanliness directly impact the system performance of not only the cathode stalk but the entirety of the SRF-PI [1]. There are four major objectives for the cathode stalk [11]. The first objective is the precision alignment control of the cathode position. The radial RF field will be biased and emittance growth will occur if the cathode position is not on center. The beam optics downstream of the SRF Gun will have difficultly recovering the emittance growth if it occurs. A second objective is to be able to bias the coaxial structure of the cathode and cathode stalk up to 5 kV DC to prevent multipacting. The third objective is temperature adjustability of the cathode which can be utilized to improve cathode performance. The fourth objective is to prevent field emission by providing a particle free cathode exchange.

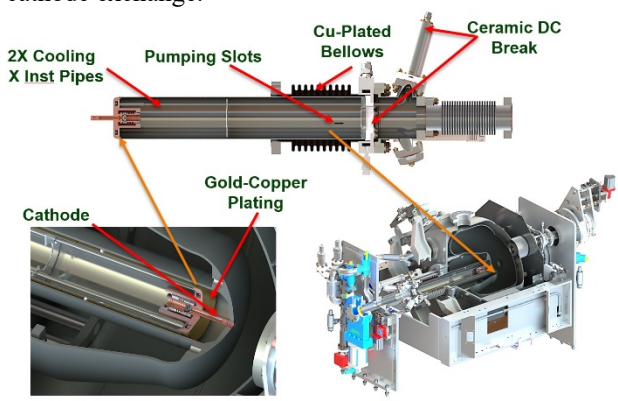

Figure 11: SRF-PI cathode stalk design and location in resonator.

Figure 11 displays the cathode stalk. The design is an adaptation previously used at HZDR [12]. The bellows flange of the cathode stalk connects to the cathode flange of the resonator. The cathode stalk tube is electrically isolated for the bellows by means of a ceramic ring. The cathode interface region is made of a copper with helium gas flow at either 55 K or 300 K. The main tube body is constructed of stainless steel which is copper and gold plated on the outside surface to reduce RF losses and thermal emissivity. The cathode tip holder sockets into a cone-shaped feature at the cathode interface area and is retained by a spring. The cathode tip holder makes surface contact which allows for conduction cooling. The DC bias is connected to the electrically isolated cooling pipes that utilized a ceramic break. Three manipulators, which mount external to the resonator, will be utilized to adjust the cathode position. This adjustment mechanism extends outside of the vacuum vessel, allowing for adjustment external to the cryomodule [11].

Coldmass Assembly

The coldmass is assembled in a cleanroom. The resonator is vented with particulate-free pure nitrogen gas after dewar testing. Particulate contamination is monitored by taking particulate count measurements on the flanges prior

ISBN: 978-3-95450-234-9 ISSN: 2673-5504 doi:10.18429/JACoW-SRF2023-FRIBA07

to connections being made on the cold string [13]. The support of the coldmass was designed using a single 316 L stainless steel welded alignment rail segment, which is annealed to relieve residual stress and restore magnetic permeability prior to precision machining. The cold string elements are fixed to the one side of alignment rail. A custom set of hardened copper bearings support the floating side of the cold string elements and allow for their differential thermal contraction. Installation of beamline bellows, FPC, RF pickup, cathode stalk, and the beamline end assemblies complete the cleanroom assembly portion of the design. Figure 12 displays the coldmass as it would be removed from the cleanroom and Figure 13 depicts a cross-section highlighting the critical components.

Figure 12: SRF-PI cryomodule coldmass. The alignment rails support the superconducting resonator and solenoid.

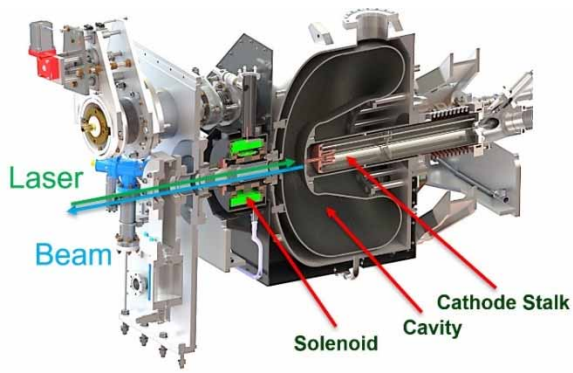

Figure 13: SRF-PI cryomodule coldmass section view displaying critical components.

On each end of the coldmass are the beamline end assemblies. These assemblies temporarily attach to the alignment rail and have a beam line vacuum connection to the resonator on the end of the coldmass string. This connection is thermally intercepted. The end assemblies allow for easy installation of gate valves, cold cathodes, and burst discs, all by ConFlat flange connections. When the coldmass is assembled with the vacuum vessel bottom plate, the end assembly is simply bolted and pinned into position and released from the end rail. Installation of the vacuum vessel cover makes an O-ring seal to the cold mass hoods which completes insulating vacuum seal.

After removal from the cleanroom, the resonator tuner, which allows for the adjustment of the resonator operating frequency is installed. Additionally, sections of the magnetic shield are installed. Once these components are installed, the coldmass is ready for installation onto the cryomodule baseplate as shown in Figure 14.

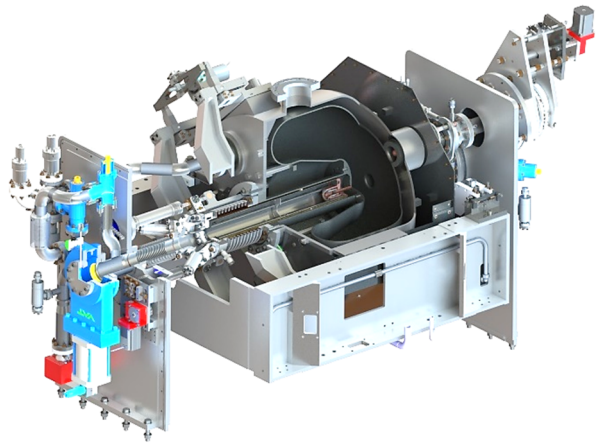

Figure 14: SRF- PI cryomodule coldmass as it is prepared for cryomodule installation – sectioned for clarification of cathode stalk components.

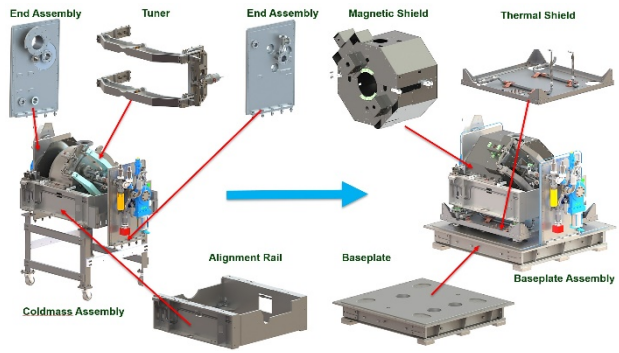

Figure 15: SRF- PI cryomodule coldmass integration for cryomodule assembly.

Magnetic Shield

The magnetic shield of the SRF-PI gun cryomodule is designed to attenuate earth's magnetic field to the resonator by 80%. This is accomplished by using a mu-metal shield for the resonator as seen in Figure 15. The magnetic shield is self-supporting off the alignment rail and is compatible with the thermal contraction of the system. The magnetic shield is designed such that accessing the tuner for maintenance at the completed cryomodule level is possible. The vacuum vessel sub-system is primarily composed of steel and further attenuates the surrounding magnetic field.

Cryogenic System

The cryogenic system has a 4 K helium circuit for the superconducting resonator, superconducting solenoid, and alignment rail. A separate 55 K helium circuit supplies the thermal shield, the FPC thermal intercept, the cathode stalk intercept, and cooling to the cathode itself. The cathode has provisions for allowing cooling at both 55 K and 300 K. The cryogenic system as installed in the cryomodule is shown in Figure 16.

ISBN: 978-3-95450-234-9 ISSN: 2673-5504 doi:10.18429/JACoW-SRF2023-FRIBA07

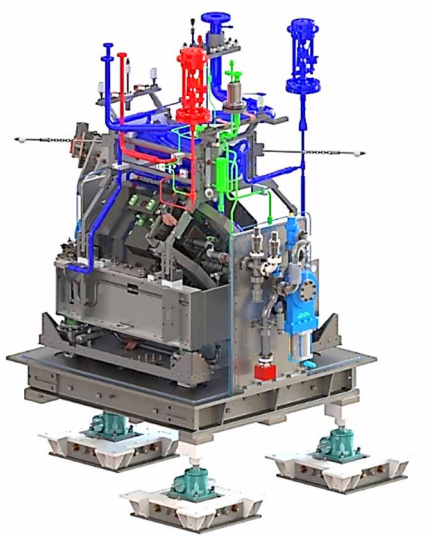

Figure 16: SRF-PI cryomodule cryogenic system installed onto the cryomodule. Blue is the 4 K circuit, red is the 55 K circuit, green is the cathode circuit.

Thermal Radiation Shield

The thermal radiation shield is a panelled construction which simplifies assembly. The thermal shield is constructed from 1100-H14 Aluminium (and cooled via a custom aluminium extrusion to distribute 55 K helium. To connect to the cryomodules's cryogenic systems, explosion bonded joints are utilized to weld the stainless steel to the aluminium. The thermal shield is supported from the G-10 alignment posts which attach to the vacuum vessel bottom plate. Figure 17 displays the installation of the thermal shield.

Vacuum Vessel and Baseplate Assembly

The vacuum vessel is constructed primarily from A36 steel. The main components are the bottom plate and vacuum vessel cover, which will interface with the hermetically sealed beamline end assemblies. Insulating vacuum space is sealed by a novel O-ring gasket which allows for simultaneous horizontal and vertical sealing. This O-ring gasket is constructed from ethylene propylene rubber more commonly known as EPDM [14]. The installation of the vacuum vessel cover is shown in Figure 17.

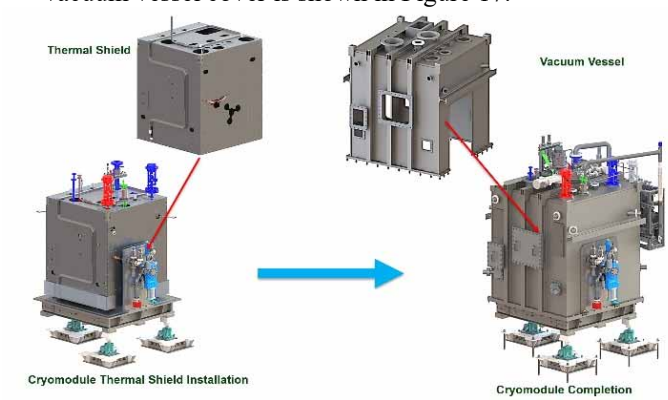

Figure 17: SRF- PI cryomodule thermal shield and vacuum vessel installation onto the cryomodule.

CRYOMODULE ASSEMBLY AND ALIGNMENT

Cryomodule Assembly

The SRF-PI cryomodule will complete final assembly at FRIB. The coldmass is installed on the cryomodule baseplate, and the subsystems are assembled to and around the coldmass. The local magnetic shield are assembled around the cavities. The cryogenic piping is installed to the coldmass via a cryogenic support structure which supports the headers and is attached to the coldmass alignment rails. The cryogenic piping is then welded to the coldmass elements. Upon verification that the cryogenic piping is leak tight, the coldmass is wrapped in multilayer insulation and then the thermal shield is installed. The thermal shield is then also wrapped with multilayer insulation. The vacuum vessel is then installed making the insulating seal of the cryomodule [14].

Cryomodule Assembly Alignment

The SRF-PI cryomodule alignment is determined by the alignment of the cathode plug aperture to the beam port aperture of the resonator. The definition and fiducialization of this line is initiated upon resonator inspection after fabrication completion. The resonator is placed on the alignment rail and gives definition to the beamline. The solenoid is adjusted to match the cavity beamline with thermal offsets being accounted for in the placement. During the cryomodule assembly stages, the beamline data is transferred to the cryomodule baseplate fiducials. It is important to control warm-to-cold offset movements during cool-down. Figure 18 displays the cryomodule thermal contraction motion.

Several key conclusions were identified during the assembly and alignment of the FRIB cryomodules. Desired structural behavior of the key components (baseplate, rails and vacuum vessel assembled to the lower subassembly) have been verified. The baseplate machined accuracy goals were reached and the baseplate can be reliably and repeatedly supported for coldmass assembly. The fixed-side hole alignment goal on the rails was achieved on the transverse component placement. The baseplate and vacuum vessel bolted assembly does perform as a rigid assembly when the adjuster mounts are manipulated and can be treated as a rigid assembly during installation. Since the same alignment/fabrication strategy is being utilized on the SRF-PI cryomodule, it is expected alignment results will be similar.

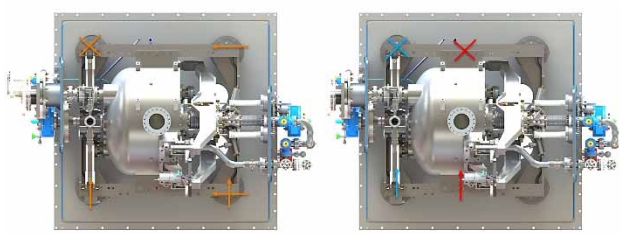

Figure 18: SRF-PI cryomodule thermal contraction motion. Thermal contraction offsets are built into the cryomodule alignment.

ISBN: 978-3-95450-234-9 ISSN: 2673-5504 doi:10.18429/JACoW-SRF2023-FRIBA07

PROJECT STATUS AND FUTURE PLANS

The project was initiated in October of 2021, with an expected completion of the cryomodule testing in early 2025. Major cryomodule components are presently in fabrication with anticipated arrival in the summer of 2023. The first superconducting resonator has completed fabrication and is currently undergoing processing in expectation of cold testing in the summer and fall of 2023. The completed cavity is shown in Figure 19. A second superconducting resonator has begun fabrication. The FPC and tuner components have also completed fabrication and will be tested in an integrated manner with the resonator. The superconducting solenoid package has the main solenoid winding complete as well as the room temperature mapping. Upon completion, the solenoid package will be cold tested prior to installation onto the coldmass.

Figure 19: SRF-PI 185.7 MHz quarter wave resonator in the electro-polishing station.

CONCLUSION

The SRF-PI cryomodule design has been completed to the performance goals and requirements. Cryomodule component fabrication is ongoing and progressing smoothly. Validation plans for critical systems are planned and proceeding where possible – with the first resonator testing in the second half of 2023.

REFERENCES

[1] LCLS-II-HE Low Emittance Injector Conceptual Design Rep. LCLSIIHE-1.1-DR-0418-R0, Mar. 13, 2022.

[2] J. W. Lewellen *et al.*, “Status of the SLAC/MSU SRF gun development project”, in *Proc. NAPAC'22*, Albuquerque, NM, USA, Aug. 2022, pp. 623-626. doi:10.18429/JACoW-NAPAC2022-WEPA03

[3] LCLS-II-HE SRF Gun Technical Specification and SOW, Rep. LCLSIIHE-1.2-TS-0206-R2, Aug. 2021.

[4] T. Xu *et al.*, “Low-emittance SRF photo-injector prototype cryomodule for the LCLS-II high-energy upgrade: design and fabrication”, presented at the IPAC'23, Venice, Italy, May 2023, paper TUPA028, to be published.

[5] S. H. Kim *et al.*, “Design of a 185.7 MHz superconducting RF photoinjector quarter-wave resonator for the LCLS-II-HE low emittance injector”, in *Proc. NAPAC'22*, Albuquerque, NM, USA, Aug. 2022, pp. 245-248. doi:10.18429/JACoW-NAPAC2022-MOPA85

[6] R. Legg *et al.*, “Wisconsin SRF gun development”, in *Proc. ERL'09*, Ithaca, NY, USA, Jun. 2009, paper WG118, pp. 45-49.

[7] M. Patil *et al.*, “Mechanical design and analysis of SRF cavity using ASME BPVC section VIII, division-2, design by analysis requirement”, presented at SRF'23, Grand Rapids, MI, USA, Jun. 2023, paper TUPTB040, this conference.

[8] X. Du *et al.*, "Design of an emittance compensation superconducting magnet package for LCLS-II-HE's SRF photoinjector," in *IEEE Trans. Appl. Supercond.*, vol. 33, no. 5, pp. 1-4, Aug. 2023, pp. 3500604. doi:10.1109/TASC.2023.3247699

[9] M.P. Kelly *et al.*, “Coaxial power coupler development at Argonne National Laboratory”, presented at SRF'17, Lanzhou, China, Jul. 2017, paper FRXBA03, unpublished.

[10] D. Passarelli, “SSR1 tuner mechanism: passive and active device”, in *Proc. LINAC'14*, Geneva, Switzerland, Aug.-Sep. 2014, paper TUPP052, pp. 541-543.

[11] T. Konomi *et al.*, “Design of the cathode stalk for the LCLS-II-HE low emittance injector”, in *Proc. NAPAC'22*, Albuquerque, NM, USA, Aug. 2022, pp. 253-255. doi:10.18429/JACoW-NAPAC2022-MOPA87

[12] R. Xiang *et al.*, “Recent improvement of Cs2Te photocathodes at HZDR”, in *Proc. IPAC'14*, Dresden, Germany, Jun. 2014, pp. 642-644. doi:10.18429/JACoW-IPAC2014-MOPRI025

[13] L. Popielarski *et al.*, “Low-Beta SRF Cavity Processing and Testing Facility for the Facility for Rare Isotope Beams at Michigan State University”, in *Proc. SRF'15*, Whistler, Canada, Sep. 2015, paper TUPB022, pp. 597-601. https://jacow.org/SRF2015/papers/TUPB022.pdf

[14] S. J. Miller *et al.*, “Low-Beta cryomodule design optimized for large-scale linac installations”, in *Proc. SRF'13*, Paris, France, Sep. 2013, paper THIOA04, pp. 825-829.